Invited Paper

UV resonance Raman signatures of phonon-allowed absorptions and phonon-driven bubble formation

Hans D. Hallen*, Adam Willitsford, Reagan Weeks, and C. Russell Philbrick

Physics Department, NC State University, Raleigh NC 27695-8202

ABSTRACT

We have measured UV resonance Raman near and at the resonance phonon-allowed absorption lines of several liquid species. Resonance absorption with excitation on the symmetry-forbidden but strongly phonon coupled bands in the 230-290 nm spectral band present enhancement corresponding to the vapor phase absorptions rather than those of the liquid phase. This effect is related to the coherence forced by the internal molecular resonance required to absorb light at this energy. Large resonance gains (~3500x) reflect the narrower vapor phase lines. At the low laser fluence used, bubble formation is observed when the excitation energy corresponds to the maximum in Raman signal generation, not at the wavelength of maximum absorption in the liquid sample, which is several nanometers away.

Keywords: Resonance Raman, Phonon-allowed Absorption, Narrow spectral features

1. INTRODUCTION

Resonance Raman typically has a pre-resonance region that spans a large excitation wavelength range [1,2,3,4,5,6,7], and the maximum resonance gain is found at the maximum absorption for the phase (liquid/gas) measured. We show that when resonance Raman is excited near a phonon-allowed absorption in liquid benzene, the situation is quite different. In particular, there is almost no pre-resonance region. Instead, a change in Raman signal level (resonance gain) by more than a factor of 3500 results from a change in excitation wavelength by 0.01 nm – in a liquid! These narrow and large magnitude resonances follow the isolated molecule (vapor phase) absorption, even though the sample is in the liquid phase. Observation of this phenomenon has been made in liquid benzene and liquid toluene [8,9,10,11,12,13]. Here, the phenomenon is investigated with a much narrower line width laser (high resolution along the excitation or resonance axis) than the previous studies, but with lower wavenumber resolution along the Raman axis (wider slit setting on the spectrometer to increase signal levels). Since this study focuses on the change in integrated Raman intensity with excitation wavelength shift, the loss of resolution along the Raman shift axis is irrelevant. The extremely narrow response requires careful measurement of the laser wavelength achieved by tuning. We insure this by referencing each scattered laser line and spectra to remnant 266 nm laser output. Very low power excitation is used to eliminate the possibility of sample damage. The small signal required larger slits on the Raman spectrometer to be used, reducing the resolution along the Raman shift axis. The vapor phase (isolated molecule) dependence of the integrated Raman signal is attributed to a limit on the interaction time imposed by the requirement of the presence of a phonon for absorption when symmetry alone does not permit it. The absorption can only happen when the nuclei are displaced from equilibrium by the phonon. This happens for a fraction of a vibration period, a time $\sim 10^{-12}$ seconds. Therefore, the process is fast, in contrast to usual expectations for resonance Raman, which has a real intermediate state. Off-resonance Raman is well known to be a very rapid process [14,15]. Since the molecule does not have time to exchange energy with its neighbors during the absorption process, the interaction appears to be that with an isolated molecule, so the resonance Raman follows the isolated molecule absorption features. The neighbor interaction time can be estimated from a comparison of the line widths (which relate in part to lifetimes or energy exchange rates) of the liquid to the isolated benzene molecule [14]. If an absorption measurement were simultaneously acquired, it would, of course, follow the liquid phase absorption, since the absorption process is not fast, so interactions with the neighbors and the long interaction time guarantees the validity of the dielectric function, which is defined in the frequency domain, a conjugate variable to time. It is somewhat surprising that a molecule in such a dense, condensed state does not realize it has neighbors, but it simply does not have the time to respond.

At resonance, a reddish glow is emitted from the laser spot in the liquid benzene. We measure this and attribute it to bubble formation driven by the laser power input. The bubble will form only long after the Raman interaction is

* Further author information: (Send correspondence to H.D.H.: E-mail: Hans_Hallen@ncsu.edu)

Ultrafast Nonlinear Imaging and Spectroscopy III, edited by Zhiwen Liu,
Proc. of SPIE Vol. 9584, 95840P · © 2015 SPIE · CCC code:
0277-786X/15/$18 · doi: 10.1117/12.2188528

complete, and emits light when the bubble bursts. Since the reddish glow appears only near resonance maxima, we suggest that the Raman process creates so many phonons (one per Raman event), and that these phonons are efficient at driving the benzene towards bubble formation, more efficiently than electronic absorption. Benzene and hydrogen emission in the UV and red part of the spectrum are observed when excitation is set to the wavelength of largest Raman resonance, as expected for excited state benzene emission (as also in plasma or flame emission studies).

2. METHODS

The tunable excitation in the deep UV spectral range is accomplished using an optical parametric oscillator (OPO) driven by a frequency-tripled Nd-YAG laser and the output of the OPO doubled to reach the UV region. The OPO uses a type II configuration with a BBO crystal, which produces a narrow laser line width (~1-2 cm^{-1}). This contrasts the ~40 cm^{-1} laser line width used in the previous studies [8,10,12]. The liquid benzene is held in a Teflon container with a silica window, and is illuminated from the bottom through the window by the excitation laser. The Raman signal is collected at 90 degrees from incidence, and the silica window is oriented so that surface reflections do not approach the spectrometer input. A short, a two stage subtractive spectrometer can be used to filter the visible wavelengths, but we leave it set to pass all wavelengths. A 1-meter spectrometer is used at 2nd order in the UV, so that the ~500 nm blazing is still optimized for the ~260 nm light used for the phonon-allowed benzene absorption. An Andor 'Newton' EM-CCD collects the Raman signal and scattered laser light.

The narrow spectral features make wavelength calibration crucial in this experiment. We use scattered laser light for this purpose. A small amount of laser light at the excitation wavelength and a small amount of remnant 266 nm (pump laser 4th harmonic are produced, since the doubling crystal following the OPO is tuned to wavelengths close to the 532 to 266 conversion) laser light is scattered and collected by the EM-CCD camera when it is tuned to the proper wavelength. The quantities that we accurately need (assuming the spectrometer is calibrated) are the number of nanometers per pixel for light incident on the CCD and the pixel value that corresponds to the set wavelength of the spectrometer. The difference wavenumbers for any pixel value can then be calculated from the excitation wavelength (measured with respect to the 266 nm light and using the nanometers per pixel), the spectrometer setting, and the nm/pixel and set pixel values. Figure 1 shows the calibration curve, which is the pixel position of the 266 nm light (center of peak) as the spectrometer is tuned to different wavelength set points. Two nm/pixel and set pixel parameters are extracted from the fit line to these data. The calibration curve is excellent, but the scatter visible on the plot means that the set-ability of the wavelength is not good enough for the 0.01 nm accuracy needed for this experiment. Therefore, for each spectrum, we collected scattered laser lines as well as Raman data, and used the spacing between the 266 nm reference signal and the tuned laser signal, along with the nm/pixel calibration, to determine the excitation wavelength rather than using the direct laser setting. This provides more accuracy on the particular wavelength set for each measurement. Typical laser power is ~7 micro-Watt average, in a spot size of ~ 5 mm^2. This ~3.5×10^{-7} W/cm^2 is low enough that we do not need to be concerned about sample damage by orders of magnitude [16,17]. The liquid holder was rotated between spectra so that fresh benzene (beyond simply replenished by self-diffusion) was used for each measurement anyway. Raman signals were integrated for 1000 seconds, and most laser line spectra for 400 seconds (although a few weaker cases required 1000 seconds).

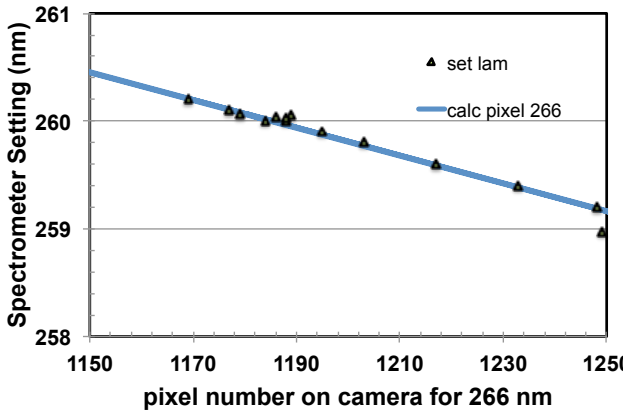

Figure 1. The calibration curve for the camera in nm/pixel and pixel value of the set point is determined by observing the position of the 266 nm 'reference' beam on the detector for different spectrometer settings.

Normally one would be concerned that the scattered laser light would swamp the detector and use layers of neutral density filters to reduce the laser signal. Figure 2 shows that this is not the case for a clean system such as this liquid one, and with the high resonance gain on the Raman signal. Raw camera outputs show that the Raman signal is actually orders of magnitude larger than the scattered laser light signal. One reason for the reduced laser scatter is that the window is oriented so that surface reflections are not directed into the spectrometer.

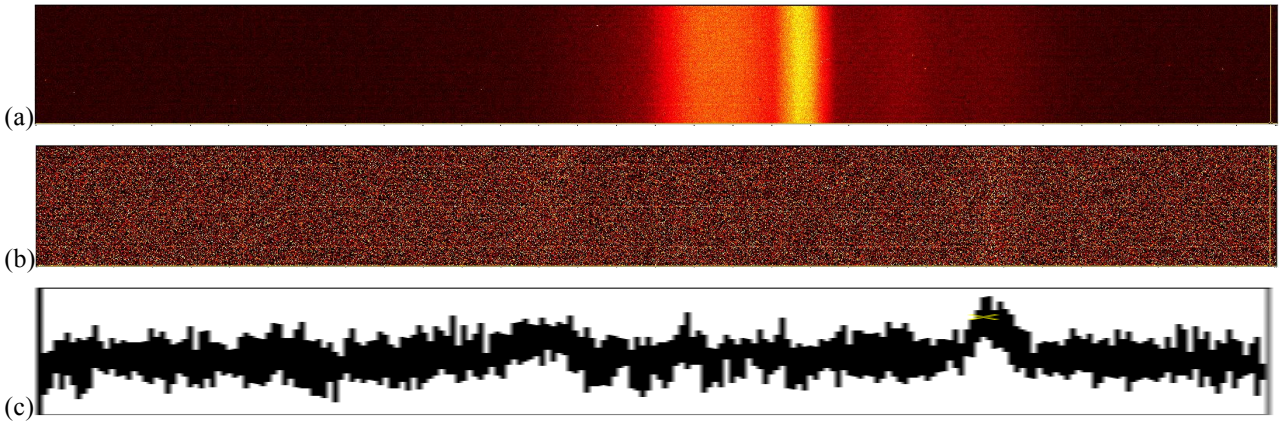

Figure 2. Raw camera outputs with xy axes are in pixels, 200 vertical and 1600 horizontal, for (a) the Raman signal at the maximum resonance with range of 275 counts (1000 s integration); the left end of the detector corresponds to 260.69 nm, and the right side to 281.32 nm. (b) The scattered laser signal with range of 27.5 counts (400 s integration) The laser signal extends form the top to the bottom of the camera output just under half-way across, and the 266 nm is about 0.8 the way to the right, both just above noise level and much weaker than the Raman signal. (c) The vertical averages of the laser scatter shown in (b) are plotted to aid observation of the lines in the image. For (b) and (c), the left side corresponds to 249.69 nm and the right side to 270.32 (20.63 nm across detection CCD).

3. RAMAN SCATTERING

We observed Raman peaks at several benzene vibration modes, similar to those observed in our previous resonant Raman studies of benzene described in the literature and referenced above, including overtones and combinations. The weak excitation and limited Raman spectral range, combined with the use of wide slits resulting in poor spectral resolution along the Raman energy axis, means that we do not observe all the vibrations. Our aim in this study is to investigate the amplitudes of the Raman signal with high resolution in the excitation energy. Observed Raman lines [18], in Herzberg notation, are $2\nu_8$ near 1400 cm^{-1}, $\nu_2+\nu_{18}$ near 1700 cm^{-1}, $2\nu_2$ near 1850 cm^{-1}, $\nu_2+\nu_{17}$ near 2000 cm^{-1}, $\nu_2+2\nu_{18}$ near 2100 cm^{-1}, $\nu_2+2\nu_8$ near 2200 cm^{-1}, and $2\nu_2+\nu_{18}$ near 2500 cm^{-1}. These peaks are similar to what has been observed before on resonance [8,9], which largely consist of replicas of the same line format with multiples of ν_2 phonons created. The $2\nu_{18}$ (added to n*the ν_2 energy) is the strongest, and has been identified as such here. The key ν_2 phonon is the ring breathing mode, which creates replicas in the absorption spectrum also, and is expected to be strongly enhanced since the ~260 nm absorption breaks a ring 'back-bond,' which should primarily impact the breathing mode. It is interesting to note that $\nu_2+2\nu_{18}$ appears only on resonance, and at different energies for each independent observation. It strongly depends upon the excited state

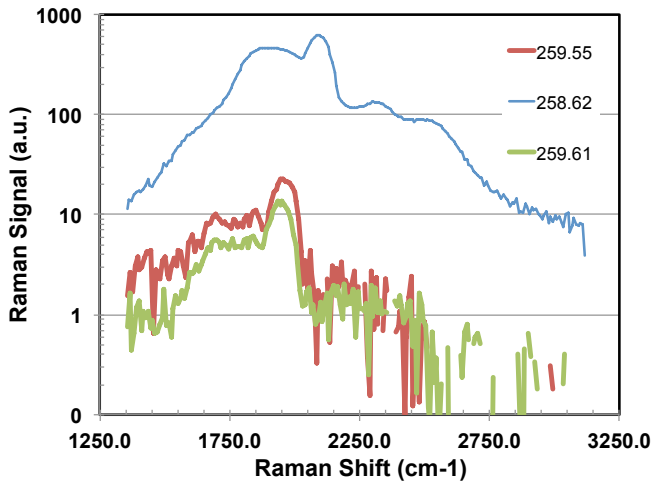

Figure 3. Raman spectra at several excitation wavelengths are shown. These spectra at 258.62, 259.55 and 259.61 are at the three main resonances found in this work. The 258.62 resonance is much stronger, so a log scale is used.

Figure 3 shows three resonant Raman spectra on a logarithmic scale, since the strongest resonance, at 258.62 nm excitation, is more than an order of magnitude larger than the other two major resonances. The spectral shapes are quite similar in the three cases, although there are different Raman energies for each case. These likely reflect slightly different excited state vibrational manifolds obtained at the different absorption features. In Fig. 4, we keep one of the resonance spectra, the smallest of the three, while displaying spectra between the main resonances. We call these non-resonant spectra. The scale is set to cut off the top of the resonance Raman spectra, which is

about 12 units, so that the features of the other spectra are more visible. They are reduced by more than another order of magnitude from the smaller resonance spectra. Again, the spectra show roughly the same vibration mode enhancement, although it is harder to discern at this scaling and signal to noise.

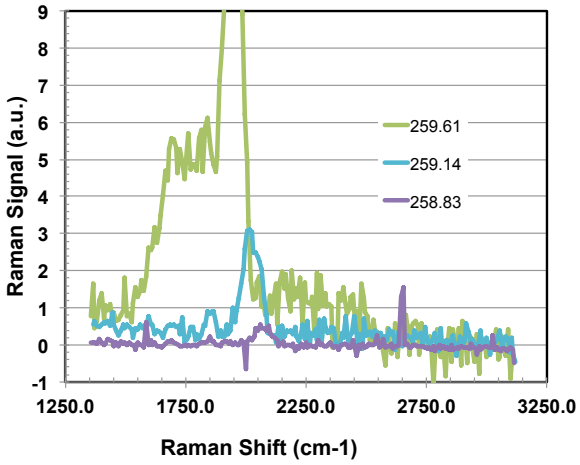

Figure 4. Raman spectra at several excitation wavelengths are shown. The spectra at 259.14 and 258.83 excitation wavelength are between the large resonances, while the spectra at 259.61 is the smallest of the three main resonances found in this work, and can be used to compare to Fig. 3.

The peak shifts between the off-resonance peaks and those on resonance are intriguing, so we plot the positions of the peaks in Fig. 5 for all observed peaks. The vibration energies show remarkably little variation away from the three resonances, with the exception of $\nu_2+\nu_{17}$, which slopes towards the peak it is a shoulder on. This effect may be due to the difficulty in identifying the peak value next to the larger peak. At the resonances, different behaviors are seen. Most observed vibration energies increase, which is opposite to both the heuristic expectation with a broken, or weakened bond, and theoretical prediction [19, but see 15 to convert Wilson to Herzberg numbering]. The latter predicts that all vibrations except the b_{2u} vibration ν_9 will decrease in energy, while that will strongly strengthen. At the strongest resonance, with 258.62 nm excitation, the $\nu_2+\nu_{18}$ weakens, while everything else strengthens. At the second resonance, at 259.55 nm excitation, the $2\nu_2+\nu_{18}$ mode is not observed, and the $\nu_2+2\nu_{18}$ is the only Raman energy that appears to be modified. At the 259.61 resonance peak, the only significant observation is the appearance of the $2\nu_2+\nu_{18}$ peak at different energies for slightly different excitation wavelengths on the resonance peak.

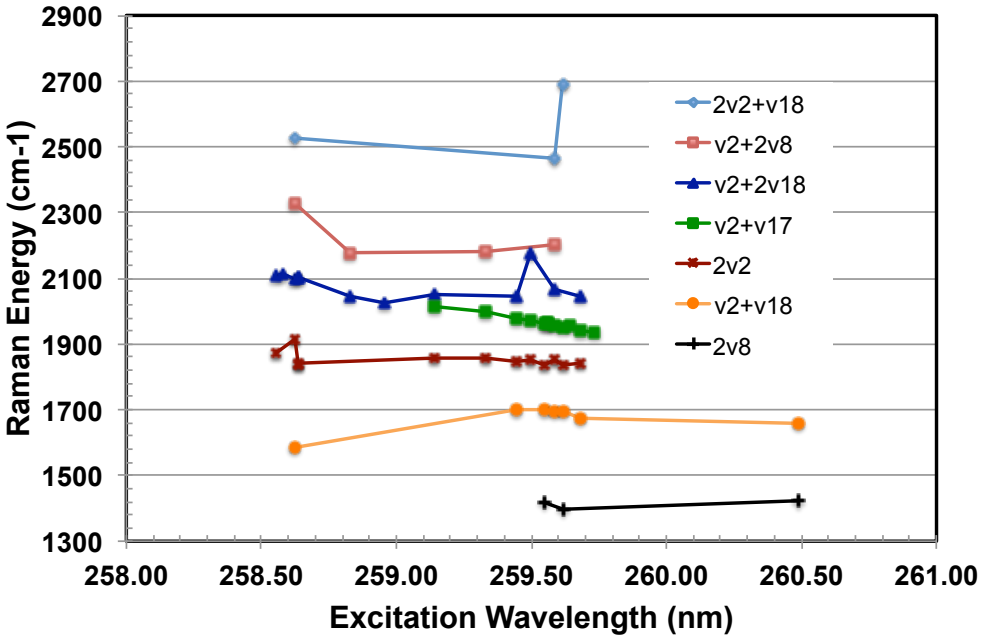

Figure 5. Raman peak energies as a function of excitation laser wavelength. Note that line at ~2000 cm^{-1}, $\nu_2+\nu_{17}$, appears as a shoulder on the stronger line at higher wavenumber shift, $\nu_2+2\nu_{18}$, so does not always appear in the chart.

The primary result of this study is the high resolution Raman signal strength measurements as the excitation wavelength is varied through the phonon-allowed absorption of benzene near 260 nm. Figure 6 shows the integral over the observed Raman peaks as a function of excitation energy.

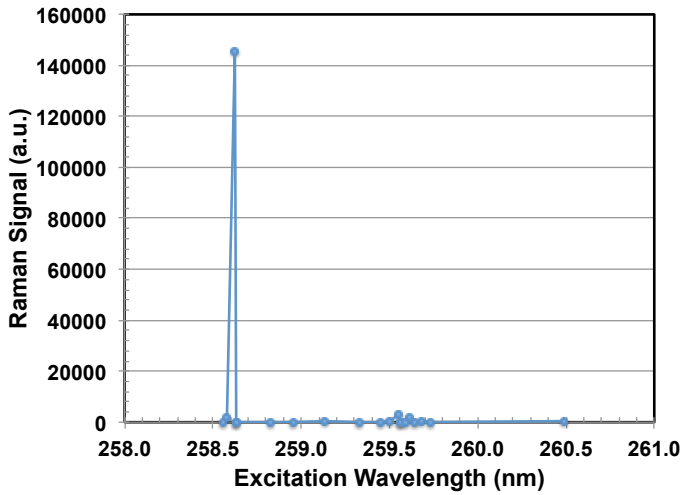

Figure 6. Integrals over the observed Raman spectra as a function of the excitation wavelength.

The most obvious observation is that the peak is very narrow. In fact, the Raman integral changes by a factor of 3500 as the excitation wavelength changes by 0.01 nm! This behavior is not typical for a condensed system, a liquid in this case. Our explanation relies on the use of a phonon-allowed (symmetry forbidden) absorption. No pre-resonance related to this absorption has been observed in previous studies of benzene pre-resonance Raman. They do, however, observe a pre-resonance to the shorter wavelength (higher energy), allowed absorption. We do not observe pre-resonance either, just a sharp resonance. Absorption at a phonon-allowed absorption requires that a phonon be present to break the symmetry of the molecule such that absorption is allowed. Thus, the molecule can only absorb while the nuclei involved are out of place. This happens for a fraction of a vibrational period, ~10^{-12} seconds. This time scale in too short for inter-molecular energy transfer, so the process is coherent, and the energy structure reflects that of an isolated molecule rather than a condensed system. The timing is controlled by the molecule (its vibration) and not by experimental conditions such as the laser pulse length (here ~7 nanoseconds).

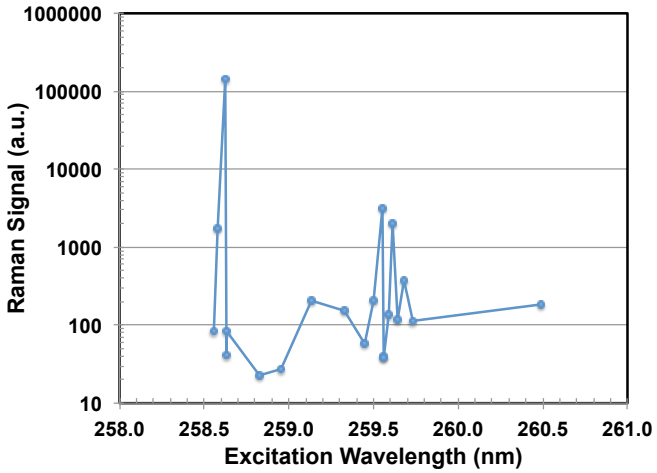

Figure 7. Integrals over the observed Raman spectra as a function of the excitation wavelength with a log scale on the vertical axis so that all parts of the spectrum show structure. Also shown is the laser intensity measured on the same camera, which is used to normalize the data.

When a logarithmic vertical scale is used, then we can observe other interesting features in Fig. 7. First, we have managed to obtain more than one point on each resonance. Interestingly, the resonances appear to be very abrupt (<0.01 nm) on the lower energy (higher wavelength) side, but more gradual on the other side, up to several hundredths of a nanometer in excitation wavelength. Next, we observe three resonances, with clear minima between. The lower level is presumably off resonant, but some structure is observed.

To understand the structure of the Raman resonance, we compare to the isolated (vapor) molecule absorption in Fig. 8. The absorption spectrum has been shifted by 1.1 nm so that the peaks line up. Note that the liquid absorption (not shown) [20,21] shows no sharp structure in this spectral region, with a broad maximum near the right edge of the plotted region. The vapor absorption data was acquired with about 2 cm^{-1} resolution. Our laser line width is narrower, so we observe a splitting compared to the absorption data in the resonances in the 256.6 nm excitation region. We also see that the rise in the background level of the integral under the Raman lines corresponds to a small peak in the absorption spectrum also. This rise is much broader than the three narrow resonances, and indicates that, although still isolated

molecule-like, the reason for the enhancement of the broader rise is likely to be physically different from that at the narrow resonances.

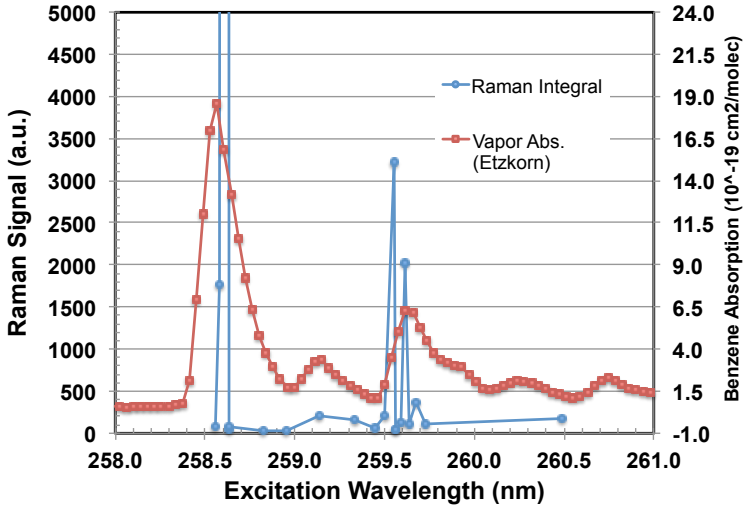

Figure 8. The integrals over the observed Raman spectra of a liquid sample as a function of the excitation wavelength are compared to the vapor phase (isolated molecule) absorption spectrum from Etzkorn [22].

We compare the prior results with a relatively broad excitation laser (bandwidth ~40 cm^{-1} = 0.27 nm) [8, 12] to these results with a narrow-band excitation laser (bandwidth ~1 cm^{-1} = 0.007 nm) in Fig. 9. In both cases, the spectra are observed to be close to zero, rising to a large value, then returning to near zero (comparatively). The data in part (a), however, is over a 2 nm excitation band while the data in (b) is over an 0.08 nm excitation band (shifted by one ring breathing mode energy in wavenumbers from that in (a)). In fact, the data in part (a) is limited by the laser line width. In contrast, we can see by the presence of some enhanced Raman intensity at 0.04 nm below the maximum in Fig. 9(b) and Figs. 7-8 that we are observing the actual molecular properties with the narrow line excitation laser. For higher excitation energy than the maximum Raman gain, the molecular response is still at least as sharp as the laser bandwidth. The asymmetric line shape is typical for threshold phenomena, which increase very rapidly once the threshold energy is reached, but the excitation is still strong above threshold. Although the plots are in terms of excitation wavelength, the conversion to energy shows that longer wavelength corresponds to lower energy.

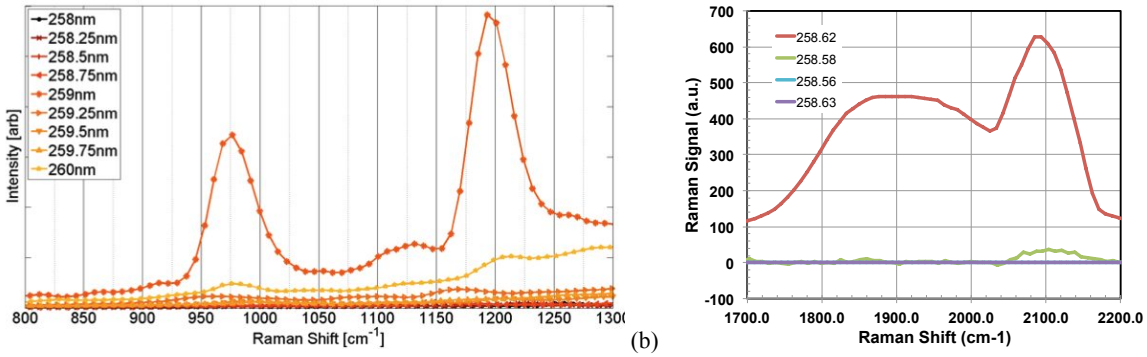

Figure 9. (a) Several Raman spectra after correction for laser power with a relatively broad laser bandwidth and 2 nm excitation range. (b) Several Raman spectra after correction for laser power with a narrow laser bandwidth and 0.08 nm band.

4. BUBBLE FORMATION

Evidence for bubble formation is a red glow from the region where the laser spot encounters the benzene. When a bubble collapses, the energy gets concentrated enough that plasma forms. The benzene molecules will break up in this

environment, and the red emission is due to the hydrogen molecular emission created by this large energy concentration when the bubble bursts. It is similar to a component of the flame emission spectra of benzene, and is expected to be around 380-385 nm and near 655 nm [23]. The red emission is shown in Fig. 10, the UV emission was measured but not shown. Our prior work also found a red emission, accompanied by an audible clicking, when the excitation wavelength was set exactly at the isolated molecule absorption peak [8]. We do not observe any audible signal since the total beam energy is much less here than in the previous study, but we do observe red emission when the excitation wavelength gives the resonance in the Raman signal. The prior work did not measure the emitted spectrum. The absorption away from the strongest Raman signal resonance is not accompanied by eventual bubble formation. The vapor-like resonance cannot have anything to do with the bubble eventually formed, as the laser pulse length is much shorter than the time it takes to form a bubble – the molecules simply cannot move fast enough to form a bubble while the laser is still within a ~7 ns long pulse. Bubble lifetimes are much shorter than the 100 ms between pulses, so bubbles created in the past will no longer be present. Thus, the bubble formation should be considered a separate process that is interesting since it occurs for a weak excitation beam at a wavelength away from the maximum in the liquid absorption, but at the wavelength of the maximum Raman resonance. The Raman process is associated with phonon creation; however, the resonance Raman results in the creation of an enormous number of phonons. This suggests that the Raman process, by directly creating phonons, couples energy more efficiently into modes that can create a bubble. The energy density of the excitation beam is also extremely small, further indicating the efficiency of the Raman-bubble energy conversion.

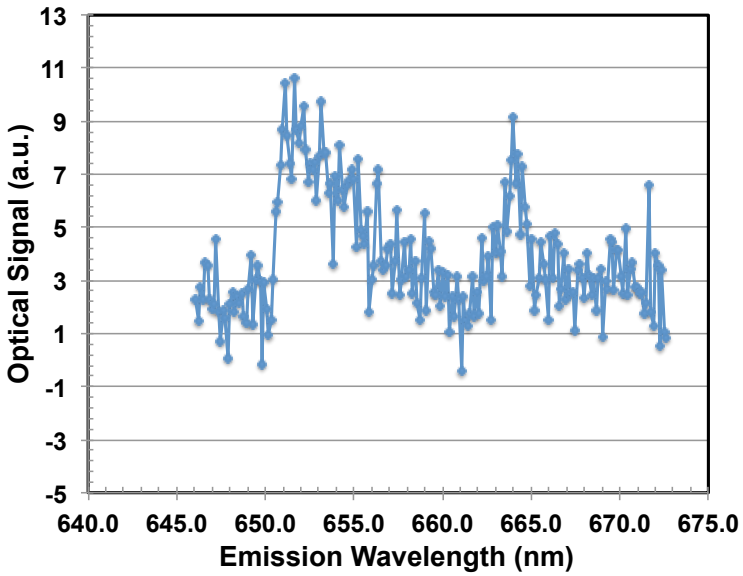

Figure 10. The emission in the red from the bursting bubble is measured with the same spectrometer as is used for the Raman data.

5. SUMMARY

The Raman signal magnitude is found to vary as the isolated benzene molecule absorption in liquid benzene as the excitation laser is tuned over the phonon-allowed, ~260 nm, B_{2u} absorption of benzene. This results in very narrow spectral features – we observed a change of 3500x in the Raman signal intensity as the excitation wavelength is changed by 0.01 nm, which is very surprising for a liquid. The explanation lies in the time domain, driven by the requirement for a phonon to be present, which forces a short duration to the absorption and Raman processes. Long after the Raman process completes, a bubble forms if the excitation wavelength is set to that which gives the largest resonance Raman signal level. Since this is not the wavelength at which the absorption length is shortest, this suggests that the phonons generated during the Raman process are more effective at creating a bubble than simple absorption in the liquid.

ACKNOWLEDGMENTS

The authors would like to thank C. Todd Chadwick, Shupeng Niu and Ling Li, all of whom aided in setting up the narrow band tunable, deep UV, laser system used in this work, and Stu Kurtz for useful discussions.

REFERENCES

1 L. Ziegler and B. Hudson, "Resonance Raman scattering of benzene and benzene-d_6 with 212.8 nm excitation," J. Chem. Phys. **74**(2), 982-992 (1981)

2 S. Asher and C. Johnson, "Resonance Raman excitation profile through the $^1B_{2u}$ state of benzene," J. Phys. Chem. **89**, 1375-1379 (1985).

3 D. Gerrity, L. Ziegler, P. Kelly, R. Desiderio, and B. Hudson, "Ultraviolet resonance Raman spectroscopy of benzene vapor with 220-184 nm excitation," J. Chem. Phys. **83**(7), 3209-3213 (1985).

4 R. Sension, R. Brudzynski, S. Li, and B. Hudson, "Resonance Raman spectroscopy of the B_{1u} region of benzene: analysis in terms of pseudo-Jahn-Teller Distortion," J. Chem. Phys. **96**(4), 2617-2628 (1991).

5 R. Sension, R. Brudzynski, and B. Hudson, "Vacuum ultraviolet resonance Raman studies of the valence electronic states of benzene and benzene-d_6: The E_{1u} state and a putative A_{2u} state," J. Chem. Phys. **94**(2), 873-882 (1990).

6 L. Ziegler and A. Albrecht, "Raman scattering of benzene in the ultraviolet," J. Chem. Phys. **67**(6), 2753-2757 (1977).

7 P. G. Harmon and S. A. Asher, "Environmental dependence of preresonance Raman cross section dispersions: Benzene vapor phase excitation profiles," J. Chem. Phys. **93**, 3094 (1990).

8 Adam Willitsford, C. Todd Chadwick, Hans Hallen, Stewart Kurtz, and C. Russell Philbrick, "Resonance Enhanced Raman Scatter in Liquid Benzene at Vapor-Phase absorption Peaks," Opt. Exp. Vol. 21, No. 22, pp. 26150–61 (2013).

9 Ling Li, Shuang Fang Lim, Alexander Puretzky, Robert Riehn, and Hans Hallen, "Near-field enhanced ultraviolet resonance Raman spectroscopy using aluminum bow-tie nano-antenna", Appl. Phys. Lett. **101** (11) Sept. 13, 2012: DOI: 10.1063/1.4746747

10 Hans D. Hallen, Shupeng Niu, and Ling Li, "Time and neighbor interaction in resonance Raman spectroscopy," Proceedings SPIE Ultrafast Imaging and Spectroscopy II, Vol. 9198, (San Diego, CA, August 17-18, 2014).

11 Hans D. Hallen, Ryan R. Neely III, Adam H. Willitsford, C. Todd Chadwick, C. Russell Philbrick, "Coherence in UV resonance Raman spectroscopy of liquid benzene and toluene, but not ice," Proceedings SPIE Ultrafast Imaging and Spectroscopy, Vol. 8845, doi: 10.1117/12.2024313 (San Diego, CA, August 25-29, 2013).

12 Adam C. Willitsford, Todd Chadwick, Hans Hallen, C. Russell Philbrick, "Resonance Raman Measurements Utilizing a Deep UV Source," in Laser Radar Technology and Applications XIIII, Proc. SPIE Vol. 6950, 8 pp. (2008).

13 C. Russell Philbrick, and Hans D. Hallen, "Laser remote sensing of species concentrations and dynamical processes," Proceedings SPIE Laser Radar Technology and Applications XIX, Vol. 9080, doi: (Baltimore, MD, May 5-9, 2014).

14 K. G. Spears, and S. A. Rice, "Study of the lifetimes of individual vibronic states of the isolated benzene molecule," J. Chem. Phys. **55**(12), 5561-5581 (1971).

15 J. H. Callomon, T. M. Dunn, I. M. Mills, "Rotational analysis of the 2600 Å absorption of benzene," Philos. Trans. R. Soc. London, Ser. A **259**(1104), 499-532 (1966).

16 S. Asher, C. Johnson, and J. Murtaugh, "Development of a new UV resonance Raman spectrometer for the 217-400 nm spectral region," Rev. Sci. Instrum. **54** (12), 1657-1662 (1983).

17 S. Asher, *Coal Liquefaction Process Streams Characterization and Evaluation UV Resonance Raman Studies of Coal Liquid Residuals*. *DOE/PC/89883-67 (DE93009669)* DOE (1993).

18 T. C. Strekas, D. H. Adams, A. Packer, and T. G. Spiro, "Absorption corrections and concentration optimization for absorbing samples in resonance Raman spectroscopy," Appl. Spectrosc. **28**(4), 324-327 (1974).

19 Yehuda Haas and Shmuel Zilberg, "The ν_{14} (b_{2u}) Mode of Benzene in S_0 and S_1 and the Distortive Nature of the π Electron System: Theory and Experiment," J. Am. Chem. Soc., vol. 117, pp. 5387-5388 (1995).

20 American Petroleum Institute Research Project 44, *Selected Ultraviolet Spectral Data* **2** (1945-1984), Thermodynamics Research Center, Department of Chemical Engineering, Texas A & M University http://catalog.lib.ncsu.edu/record/NCSU623743

21 J. M. Dixon, M. Taniguchi, and J. S. Lindsey, "PhotochemCAD 2: A refined program with accompanying spectral databases for photochemical calculations," Photochem. Photobiol. **81**, 212-213 (2005) http://omlc.ogi.edu/spectra/PhotochemCAD/html/042.html (benzene) http://omlc.ogi.edu/spectra/PhotochemCAD/html/090.html (toluene).

22 T. Etzkorn, B. Klotz, S. Sørensen, I. V. Patroescu, I. Barnes, K. H. Becker, and U. Platt, "Gas-phase absorption cross sections of 24 monocyclic aromatic hydrocarbons in the UV and IR spectral ranges,"Atmos. Environ. **33**, 525-540 (1999), *MPI-Mainz-UV-VIS Spectral Atlas of Gaseous Molecules* http://www.satellite.mpic.de/spectral_atlas.org

23 S. J. Mousavi, M. Hemati Farsani, S. M. R. Darbani, N. Asadorian, M. Soltanolkotabi, and A. Eslami Majd "Identification of atomic lines and molecular bands of benzene and carbon disulfide liquids by using LIBS,"*Applied Optics*, Vol. **54**, No. 7, pp. 1713-1720 (2015) , doi: 10.1364/AO.54.001713.